Supporting Information

Preferential Activation of CO near Hydrocarbon Chains during Fischer-Tropsch Synthesis on Ru

David Hibbitts[a,b], Eric Dybeck[c], Thomas Lawlor[c], Matthew Neurock[c,d*], and Enrique Iglesia[a*]

[a] Department of Chemical and Biomolecular Engineering, University of California, Berkeley, CA, 94720, United States
[b] Present Address: Department of Chemical Engineering, University of Florida, Gainesville, FL, 32611, United States
[c] Department of Chemical Engineering, University of Virginia, Charlottesville, VA, 22904, United States
[d] Department of Chemical Engineering and Materials Science, University of Minnesota, Minneapolis, MN, 55455, United States
* Corresponding authors. iglesia@berkeley.edu (E. Iglesia) and mneurock@umn.edu (M. Neurock).

Table of Contents

List of Figures and Tables

S1. Details of DFT calculations of thermochemical properties

Frequency calculations were carried out on all optimized states to determine zero-point vibrational energies (*ZPVE*), vibrational enthalpies (H_{vib}), and free energies (G_{vib}). Their values were used, together with VASP-derived electronic energies (E_0), to obtain enthalpies:

$$H = E_0 + ZPVE + H_{vib} + H_{trans} + H_{rot} \tag{S1}$$

and free energies:

$$G = E_0 + ZPVE + G_{vib} + G_{trans} + G_{rot} \tag{S2}$$

for all reactant, product, and transition state structures. For RPBE GGA, the dispersion-corrected enthalpies:

$$H = E_0 + E_d + ZPVE + H_{vib} + H_{trans} + H_{rot} \tag{S3}$$

and free energies:

$$G = E_0 + E_d + ZPVE + G_{vib} + G_{trans} + G_{rot} \tag{S4}$$

Entropy can be determined for a state with a known *H* and *G* at a given *T*:

$$S = \frac{H - G}{T} \tag{S5}$$

For calculations which include the Ru_{218} catalyst model (including adsorbed species and transition states on that surface), there are no translational or rotational degrees of freedom and DFT-derived vibrational frequencies can be used to determine the *ZPVE*, H_{vib} and G_{vib} shown in Eqns. S6-8.

$$ZPVE = \sum_i (\tfrac{1}{2} v_i h) \tag{S6}$$

$$H_{vib} = \sum_i \left(\frac{v_i h e^{\frac{-v_i h}{kT}}}{1 - e^{\frac{-v_i h}{kT}}} \right) \tag{S7}$$

$$G_{vib} = \sum_i \left(-kT \ln \frac{1}{1 - e^{\frac{-v_i h}{kT}}} \right) \tag{S8}$$

where v_i is the frequency, *h* is Planck's constant, *k* is Boltzmann's constant.

Gas-phase molecules have translational and rotational degrees of freedom; thus H_{trans}, H_{rot}, G_{trans} and G_{rot} must also be computed: [1]

$$H_{trans} = \frac{5}{2} kT \tag{S9}$$

$$H_{rot,linear} = kT \tag{S10}$$

$$G_{trans} = -kT \ln\left[\left(\frac{2\pi MkT}{h^2}\right)^{3/2} V\right] \tag{S11}$$

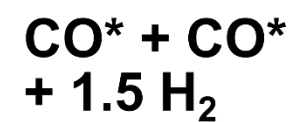$$G_{rot} = -kT \ln\left[\frac{\pi^{1/2}}{\sigma}\left(\frac{T^3}{\theta_x\theta_y\theta_z}\right)^{1/2}\right] \tag{S12}$$

$$\theta_i = \frac{h^2}{8\pi^2 I_i k} \tag{S13}$$

where I_i is the moment of inertia about axes x, y or z and σ is the symmetry number of the molecule, 2 for H_2, 1 for CO, 2 for H_2O.

[1] Statistical Mechanics", D. A. McQuarrie, 2000, University Science Books, Sausolito, CA.

S2. Summary of DFT-derived structures and geometries

CO* + CO* + 1.5 H$_2$

ΔH(kJ mol^{-1})   **0**
ΔS (J mol^{-1} K^{-1})   **0**
ΔG(kJ mol^{-1})   **0**

CO* + * + CO + 1.5 H$_2$
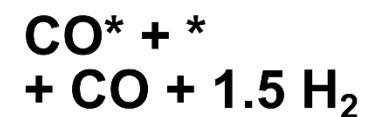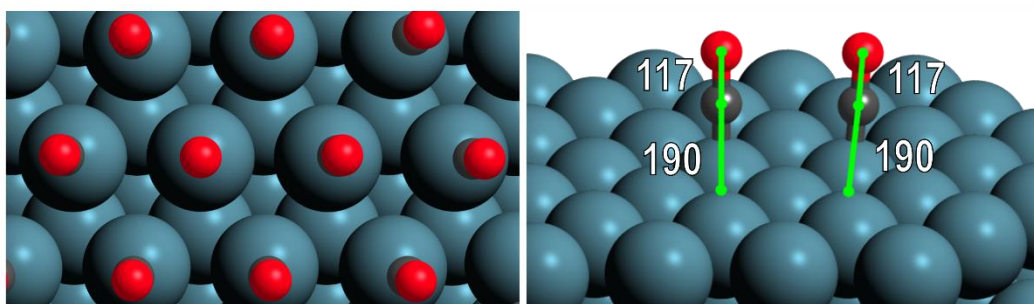
ΔH(kJ mol^{-1})   **104**
ΔS (J mol^{-1} K^{-1})   **165**
ΔG(kJ mol^{-1})   **22**

Figure S1. DFT-derived structures (top-down view (left) and side-on view (right) without spectator CO* for clarity) for CO* desorption. The ΔH (kJ mol^{-1}), ΔS (J mol^{-1} K^{-1}), and ΔG (kJ mol^{-1}) required to form the vacancy from a CO*-covered surface is shown on the left. Other energy-differences shown in Table S1.

CO* + H'
+ CO + 1.0 H$_2$

ΔH(kJ mol^{-1})	**97**
ΔS (J mol^{-1} K^{-1})	**95**
ΔG(kJ mol^{-1})	**60**

H–C*O*‡
+ CO + 1.0 H$_2$

ΔH(kJ mol^{-1})	**189**
ΔS (J mol^{-1} K^{-1})	**77**
ΔG(kJ mol^{-1})	**150**

CH*O*
+ CO + 1.0 H$_2$

ΔH(kJ mol^{-1})	**176**
ΔS (J mol^{-1} K^{-1})	**89**
ΔG(kJ mol^{-1})	**131**

Figure S2. DFT-derived structures (top-down view (left) and side-on view (right) without spectator CO* for clarity) for CH*O* formation. The ΔH (kJ mol^{-1}), ΔS (J mol^{-1} K^{-1}), and ΔG (kJ mol^{-1}) required to form each state from a CO*-covered surface is shown on the left. Other energy-differences shown in Table S1. Notable bond distances shown in pm.

CH*O* + H'
+ CO + 0.5 H$_2$

ΔH(kJ mol^{-1})   **172**
ΔS (J mol^{-1} K^{-1})   **20**
ΔG(kJ mol^{-1})   **162**

CH*O*–H$\neq$
+ CO + 0.5 H$_2$

ΔH(kJ mol^{-1})   **234**
ΔS (J mol^{-1} K^{-1})   **10**
ΔG(kJ mol^{-1})   **228**

CH*OH*
+ CO + 0.5 H$_2$

ΔH(kJ mol^{-1})   **182**
ΔS (J mol^{-1} K^{-1})   **18**
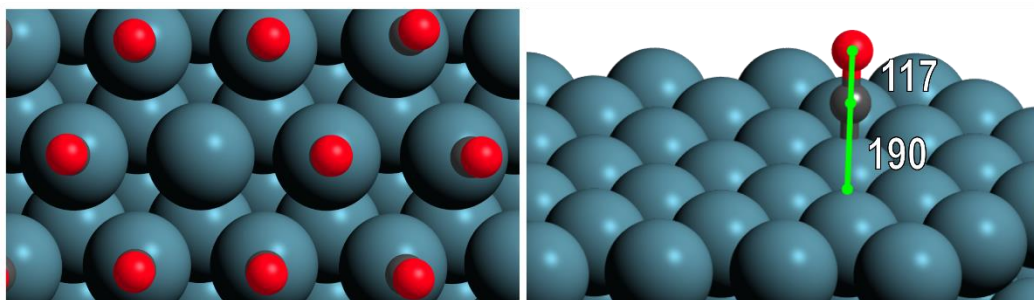ΔG(kJ mol^{-1})   **173**

Figure S3. DFT-derived structures (top-down view (left) and side-on view (right) without spectator CO* for clarity) for CH*OH* formation. The ΔH (kJ mol^{-1}), ΔS (J mol^{-1} K^{-1}), and ΔG (kJ mol^{-1}) required to form each state from a CO*-covered surface is shown on the left. Other energy-differences shown in Table S1. Notable bond distances shown in pm.
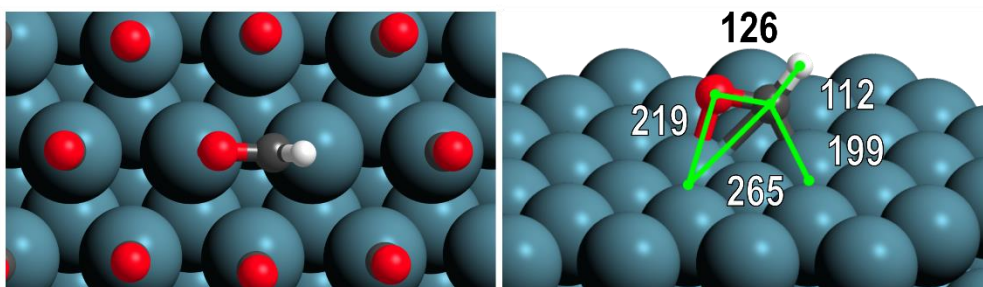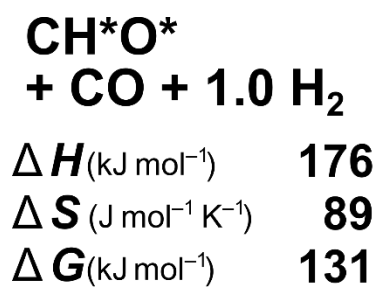
7

CH*OH*
+ CO + 0.5 H$_2$

ΔH(kJ mol^{-1})   **182**
ΔS (J mol^{-1} K^{-1})   **18**
ΔG(kJ mol^{-1})   **173**

CH*–OH*$\neq$
+ CO + 0.5 H$_2$

ΔH(kJ mol^{-1})   **233**
ΔS (J mol^{-1} K^{-1})   **15**
ΔG(kJ mol^{-1})   **225**

CH* + OH*
+ CO + 0.5 H$_2$

ΔH(kJ mol^{-1})   **155**
ΔS (J mol^{-1} K^{-1})   **36**
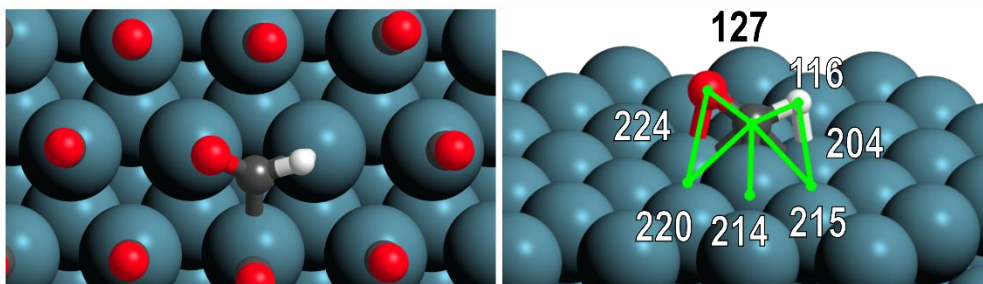ΔG(kJ mol^{-1})   **137**

Figure S4. DFT-derived structures (top-down view (left) and side-on view (right) without spectator CO* for clarity) for CH*OH* dissociation. The ΔH (kJ mol^{-1}), ΔS (J mol^{-1} K^{-1}), and ΔG (kJ mol^{-1}) required to form each state from a CO*-covered surface is shown on the left. Other energy-differences shown in Table S1. Notable bond distances shown in pm.
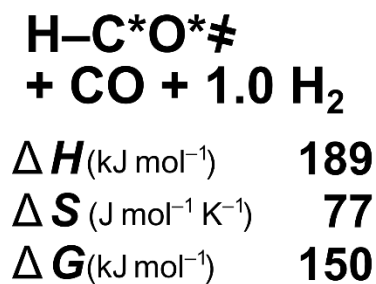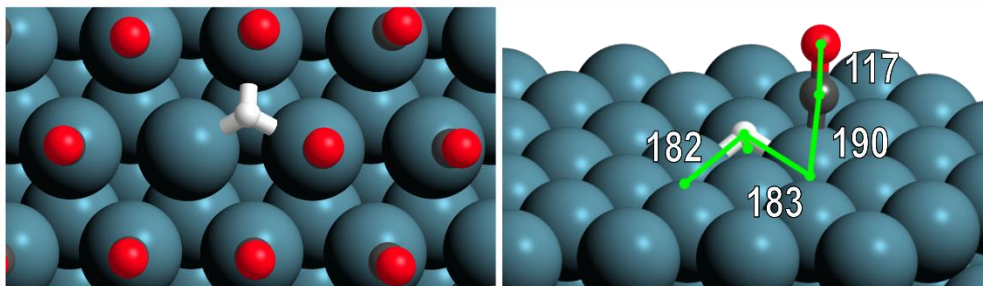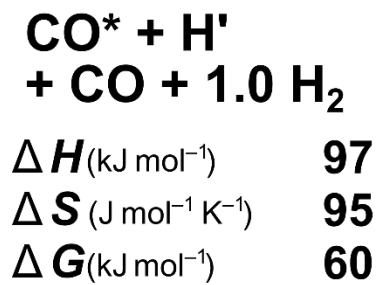
8

CH* + OH* + H'
+ CO

ΔH (kJ mol^{-1})   **159**
ΔS (J mol^{-1} K^{-1})   **−39**
ΔG (kJ mol^{-1})   **178**

CH* + OH*–H≠
+ CO

ΔH (kJ mol^{-1})   **175**
ΔS (J mol^{-1} K^{-1})   **−51**
ΔG (kJ mol^{-1})   **200**

CH* + *
+ CO + H$_2$O

ΔH (kJ mol^{-1})   **95**
ΔS (J mol^{-1} K^{-1})   **122**
ΔG (kJ mol^{-1})   **34**

CH* + CO*
+ H$_2$O

ΔH (kJ mol^{-1})   **−23**
ΔS (J mol^{-1} K^{-1})   **−41**
ΔG (kJ mol^{-1})   **−2**

Figure S5. DFT-derived structures (top-down view (left) and side-on view (right) without spectator CO* for clarity) for H$_2$O formation and CO* re-adsorption. The ΔH (kJ mol^{-1}), ΔS (J mol^{-1} K^{-1}), and ΔG (kJ mol^{-1}) required to form each state from a CO*-covered surface is shown on the left. Other energy-differences shown in Table S1. Notable bond distances shown in pm.
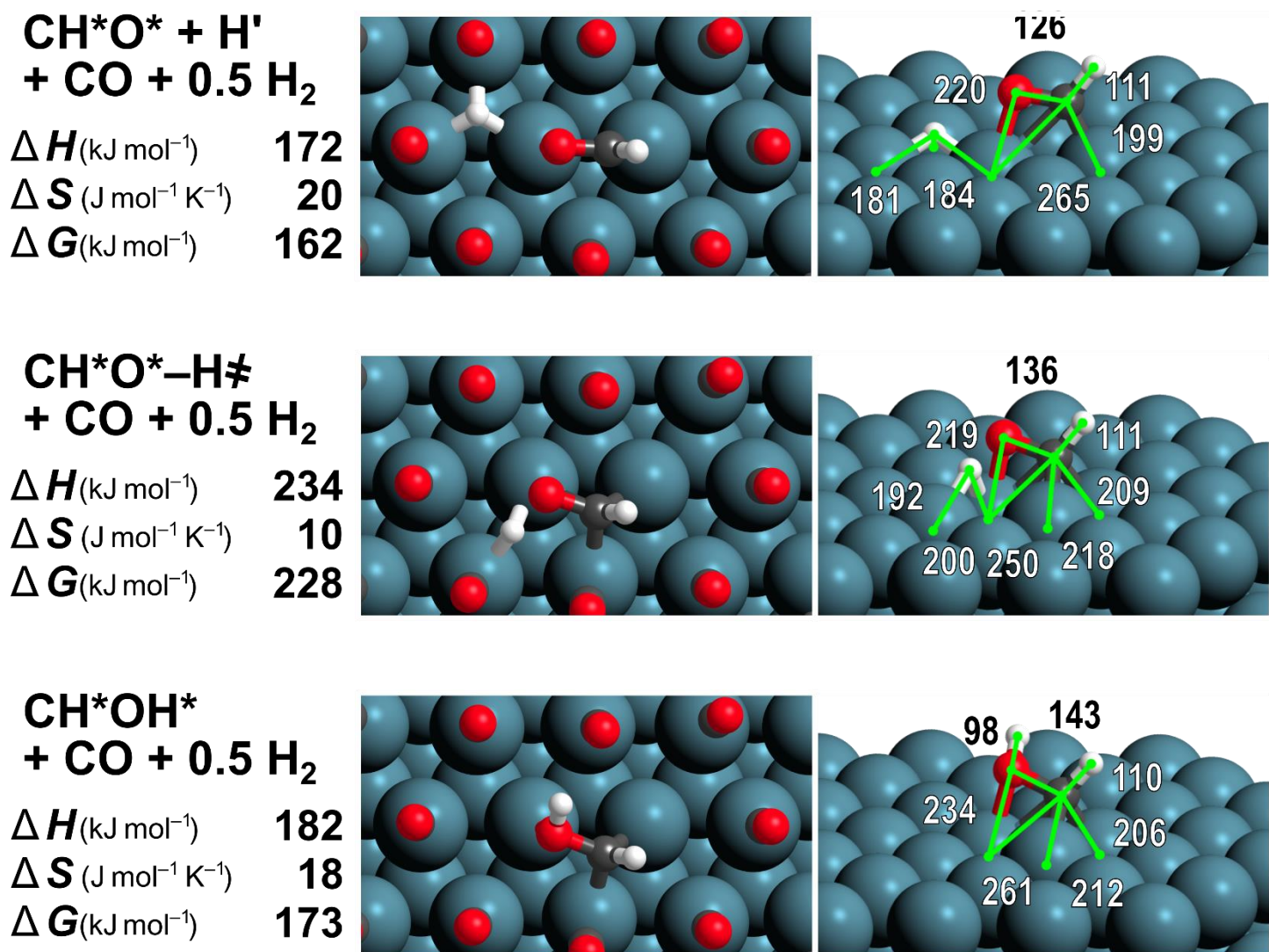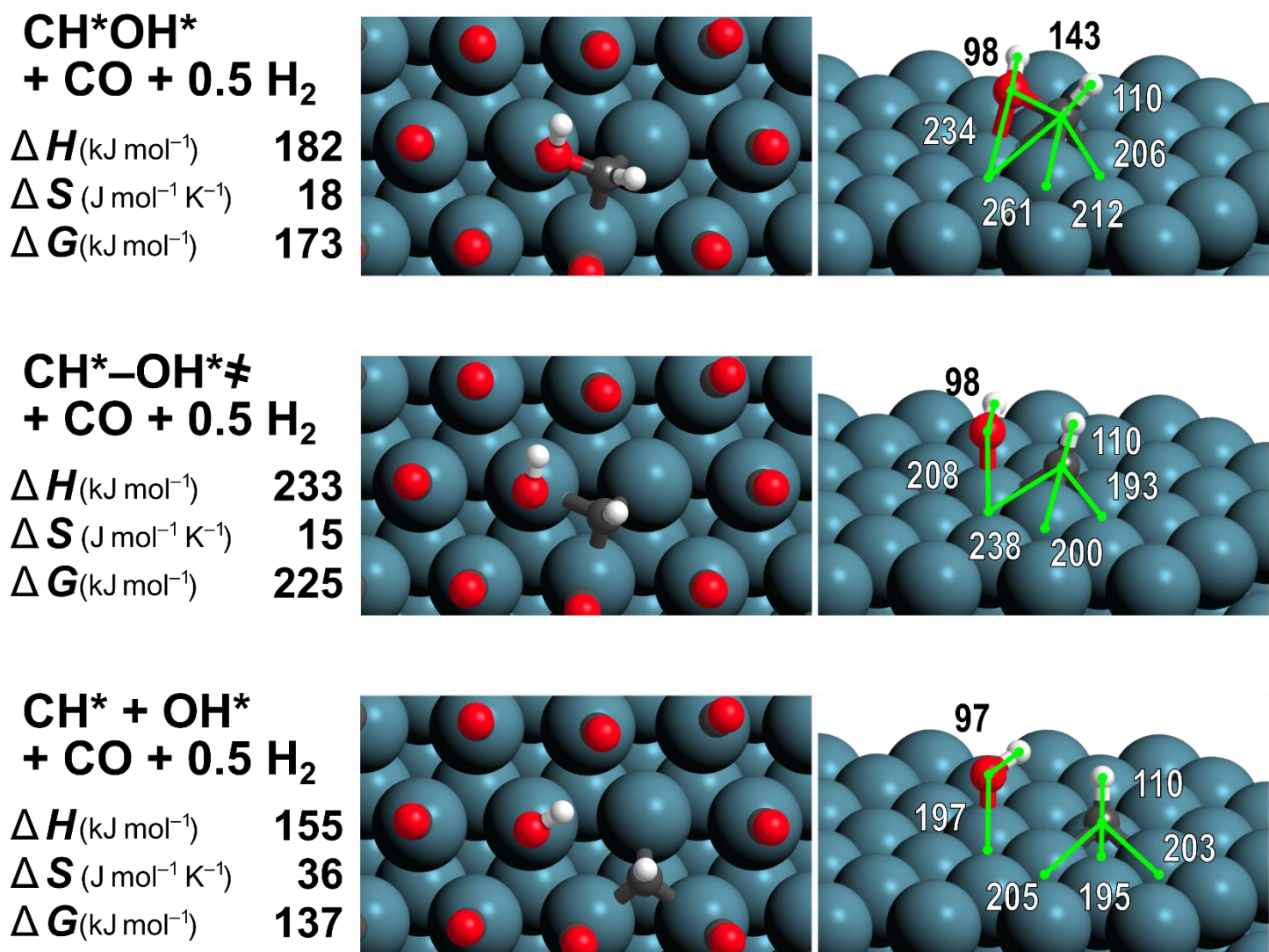
CO* + CH*
+ 1.5 H₂

ΔH (kJ mol⁻¹)	0
ΔS (J mol⁻¹ K⁻¹)	0
ΔG (kJ mol⁻¹)	0

CO* + H' + CH*
+ 1.0 H₂

ΔH (kJ mol⁻¹)	−2
ΔS (J mol⁻¹ K⁻¹)	−68
ΔG (kJ mol⁻¹)	31

H–C*O*≠ + CH'
+ 1.0 H₂

ΔH (kJ mol⁻¹)	106
ΔS (J mol⁻¹ K⁻¹)	−88
ΔG (kJ mol⁻¹)	151

CH*O* + CH'
+ 1.0 H₂

ΔH (kJ mol⁻¹)	65
ΔS (J mol⁻¹ K⁻¹)	−76
ΔG (kJ mol⁻¹)	103

Figure S6. DFT-derived structures (top-down view (left) and side-on view (right) without spectator CO* for clarity) for CH*O* formation vicinal to a CH' chain. The ΔH (kJ mol⁻¹), ΔS (J mol⁻¹ K⁻¹), and ΔG (kJ mol⁻¹) required to form each state from a CO*-covered surface is shown on the left. Other energy-differences shown in Table S2. Notable bond distances shown in pm.
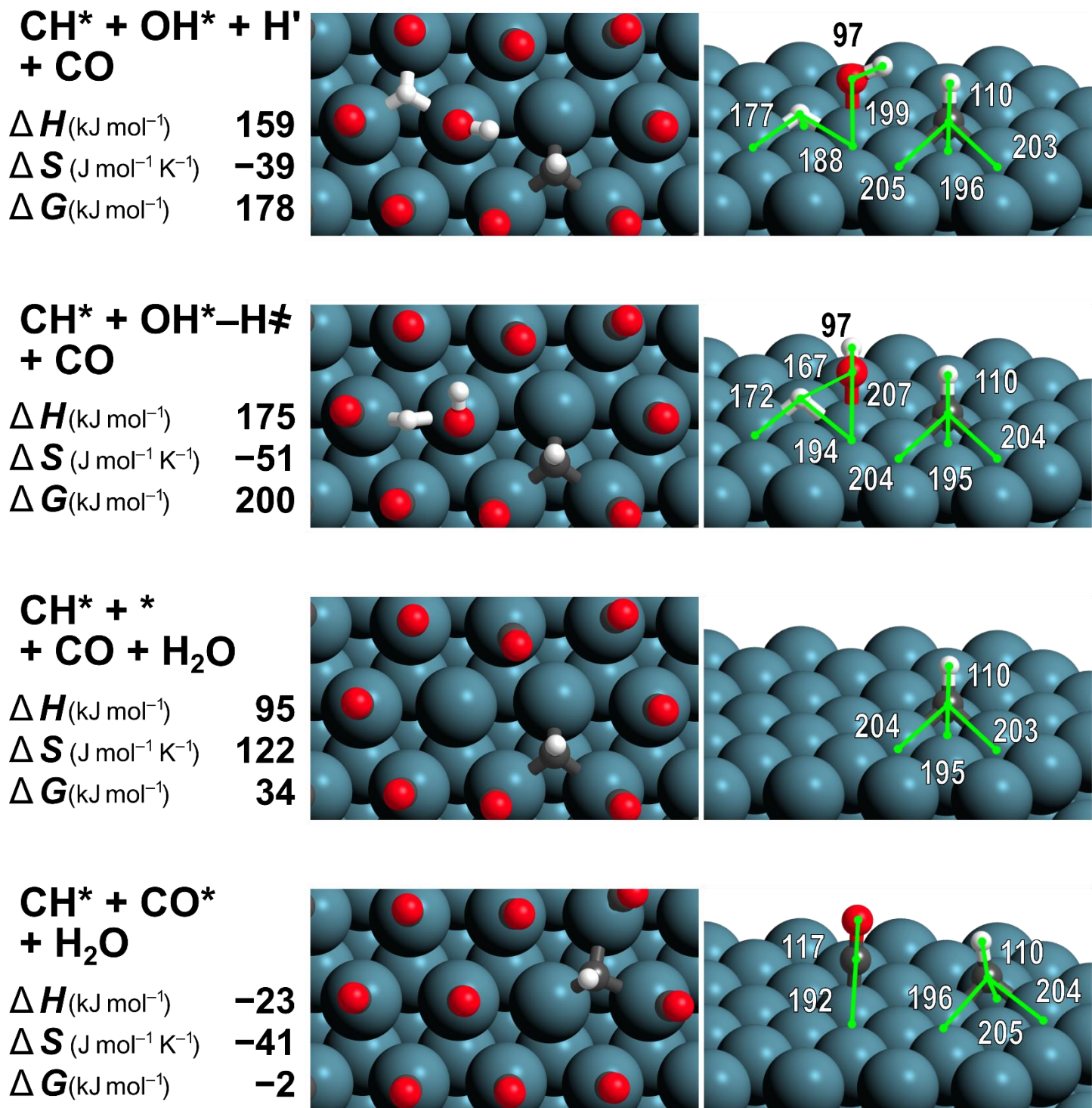
**CH*O* + H' + CH'
+ 0.5 H$_2$**

ΔH(kJ mol^{-1})	68
ΔS (J mol^{-1} K^{-1})	−145
ΔG(kJ mol^{-1})	140

**CH*O*–H≠ + CH'
+ 0.5 H$_2$**

ΔH(kJ mol^{-1})	127
ΔS (J mol^{-1} K^{-1})	−155
ΔG(kJ mol^{-1})	204

**CH*OH* + CH'
+ 0.5 H$_2$**
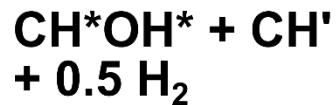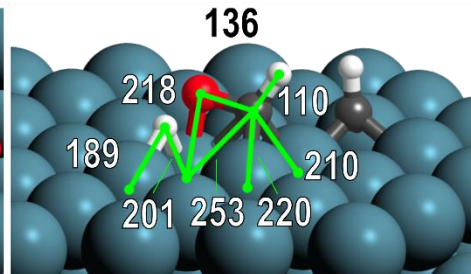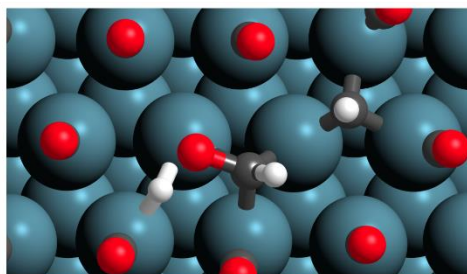
ΔH(kJ mol^{-1})	72
ΔS (J mol^{-1} K^{-1})	−147
ΔG(kJ mol^{-1})	145

Figure S7. DFT-derived structures (top-down view (left) and side-on view (right) without spectator CO* for clarity) for CH*OH* formation vicinal to a CH' chain. The ΔH (kJ mol^{-1}), ΔS (J mol^{-1} K^{-1}), and ΔG (kJ mol^{-1}) required to form each state from a CO*-covered surface is shown on the left. Other energy-differences shown in Table S2. Notable bond distances shown in pm.
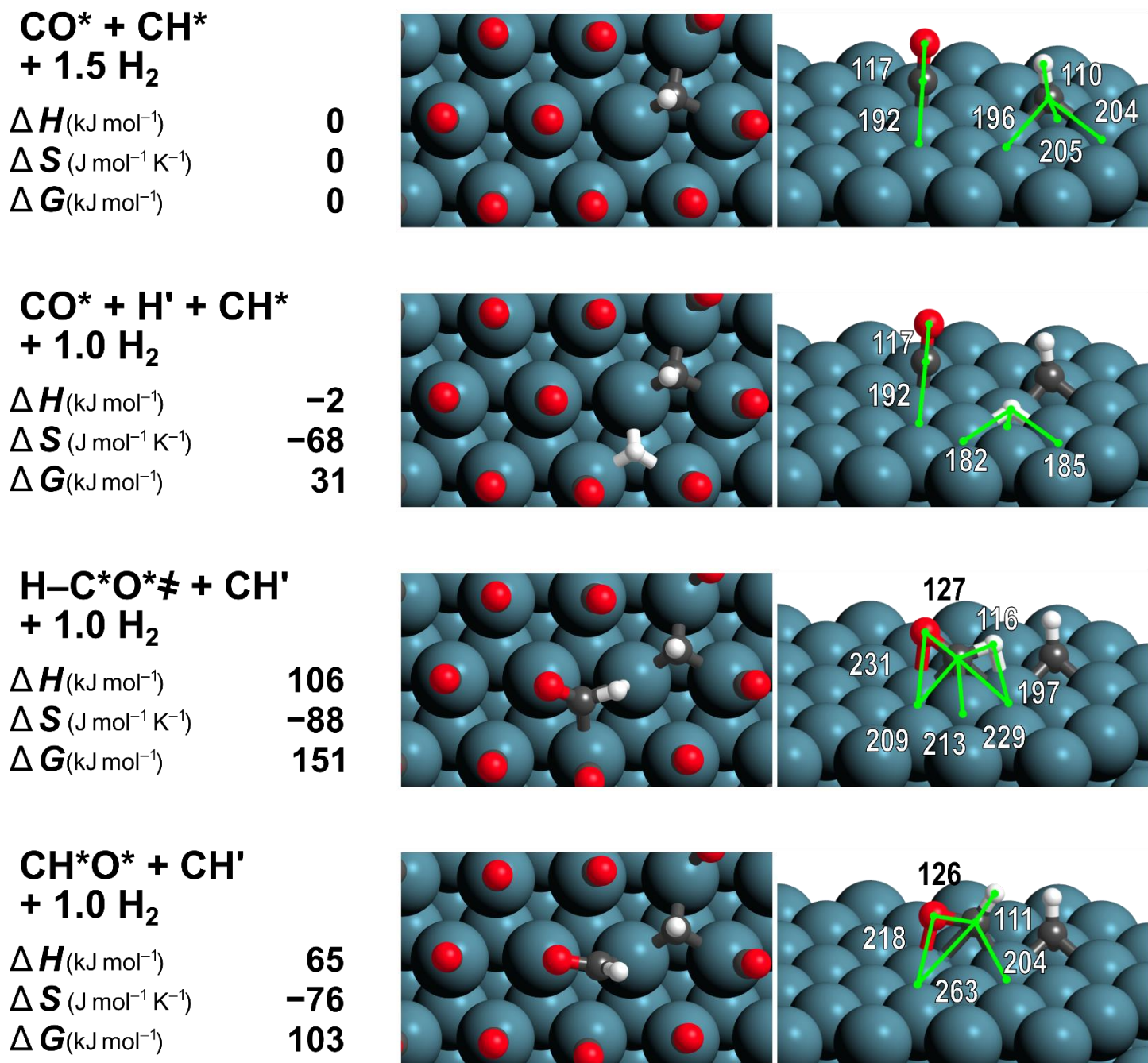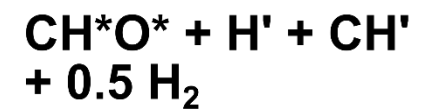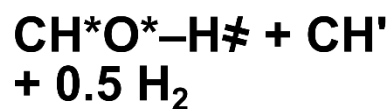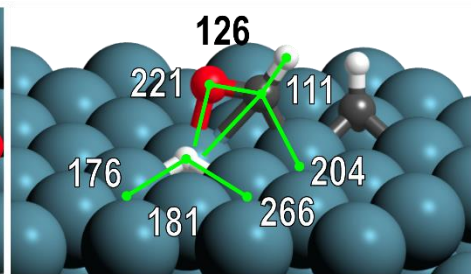
CH*OH* + CH'
+ 0.5 H$_2$

ΔH(kJ mol^{-1})   72
ΔS (J mol^{-1} K^{-1})   −147
ΔG(kJ mol^{-1})   145

CH*−OH*‡ + CH'
+ 0.5 H$_2$

ΔH(kJ mol^{-1})   129
ΔS (J mol^{-1} K^{-1})   −144
ΔG(kJ mol^{-1})   201

CH* + OH* + CH'
+ 0.5 H$_2$

ΔH(kJ mol^{-1})   68
ΔS (J mol^{-1} K^{-1})   −133
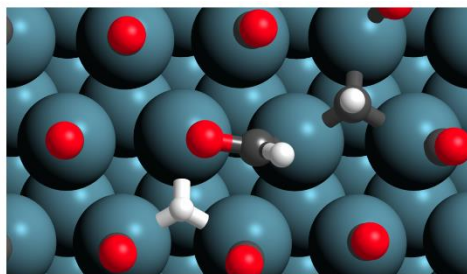ΔG(kJ mol^{-1})   135
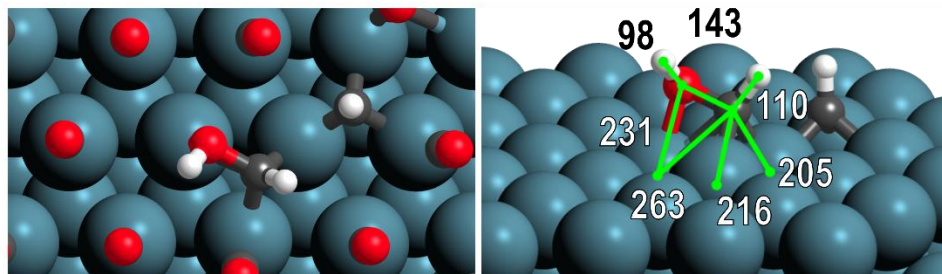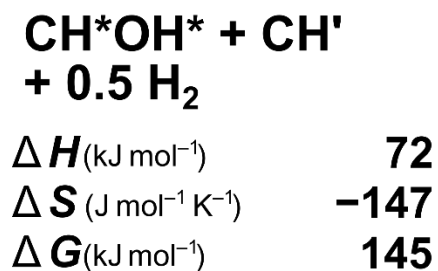
Figure S8. DFT-derived structures (top-down view (left) and side-on view (right) without spectator CO* for clarity) for CH*OH* dissociation vicinal to a CH' chain. The ΔH (kJ mol^{-1}), ΔS (J mol^{-1} K^{-1}), and ΔG (kJ mol^{-1}) required to form each state from a CO*-covered surface is shown on the left. Other energy-differences shown in Table S2. Notable bond distances shown in pm.

CH* + OH* + H' + CH'

ΔH (kJ mol^{-1})	72
ΔS (J mol^{-1} K^{-1})	−206
ΔG (kJ mol^{-1})	176

CH* + OH*–H≠ + CH'

ΔH (kJ mol^{-1})	93
ΔS (J mol^{-1} K^{-1})	−214
ΔG (kJ mol^{-1})	200

CH* + * + CH' + H$_2$O

ΔH (kJ mol^{-1})	12
ΔS (J mol^{-1} K^{-1})	−47
ΔG (kJ mol^{-1})	35

CH* + CO* + CH' + H$_2$O

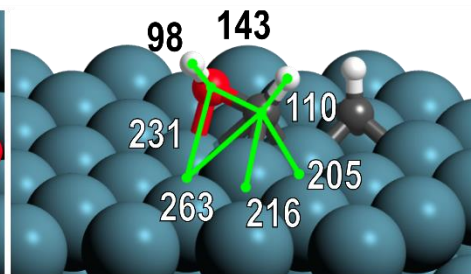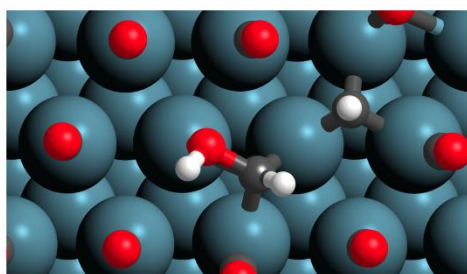|	
ΔH (kJ mol^{-1})	−104
ΔS (J mol^{-1} K^{-1})	−211
ΔG (kJ mol^{-1})	2

Figure S9. DFT-derived structures (top-down view (left) and side-on view (right) without spectator CO* for clarity) for H$_2$O formation and CO* re-adsorption vicinal to a CH' chain. The ΔH (kJ mol^{-1}), ΔS (J mol^{-1} K^{-1}), and ΔG (kJ mol^{-1}) required to form each state from a CO*-covered surface is shown on the left. Other energy-differences shown in Table S2. Notable bond distances shown in pm.
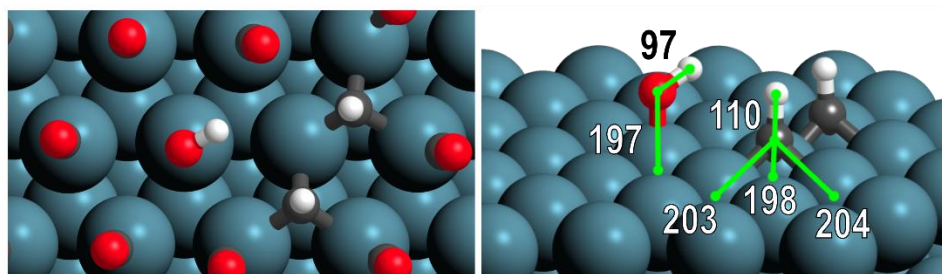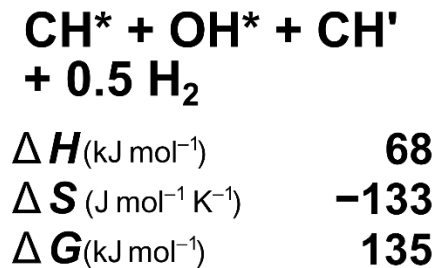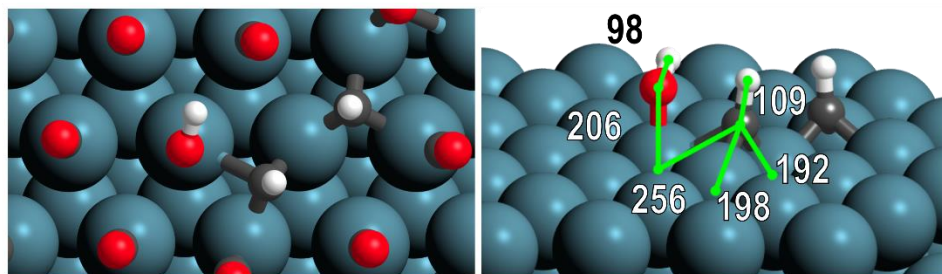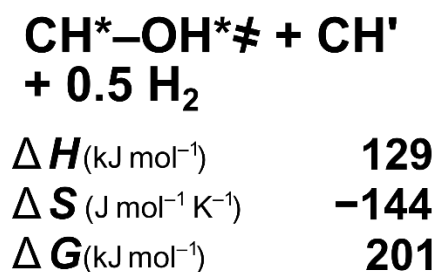
13

S3. Differences in CO* activation free energies with and without vicinal CH* predicted by different DFT functionals

Table R1. Adsorption free energies for CO* and effective free energy barriers for activating CO* with ($\Delta G_1^{\ddagger}$) and without ($\Delta G_0^{\ddagger}$) a vicinal CH*.

		$\Delta G_{ads,CO}$	$\Delta G_0^{\ddagger}$	$\Delta G_1^{\ddagger}$	$\Delta G_0^{\ddagger} - \Delta G_1^{\ddagger}$
		kJ mol^{-1}	kJ mol^{-1}	kJ mol^{-1}	kJ mol^{-1}
RPBE	PAW	+36	199	229	−30
RPBE-D3	PAW	−84	262	196	66
RPBE-D3(NMI)	PAW	−22	228	204	24
PW91	USPP	−18	209	179	30
optB86b-vdW	PAW	−55	224	186	38
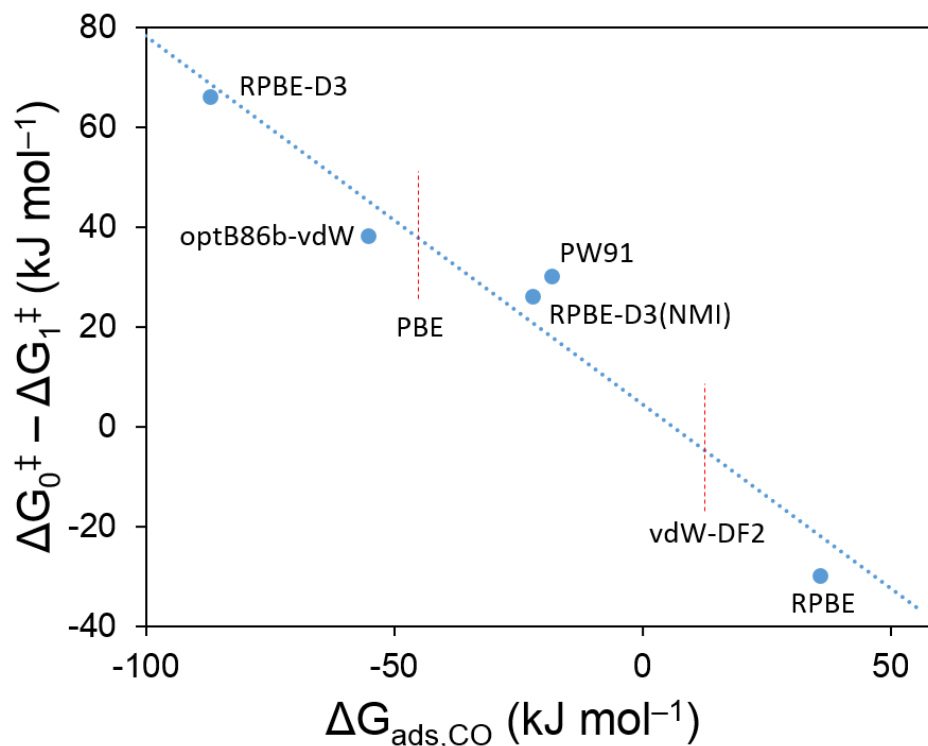
Figure S10. Difference between the effective free energy barrier for CO* activation vicinal to a CH* fragment ($\Delta G_{\gamma 1}^{\ddagger}$) and without a nearby alkylidyne chain ($\Delta G_{\gamma 0}^{\ddagger}$). Vertical dashed lines show the functionals for which the $\Delta G_{ads,CO}$ was computed but not the free energy barriers for CO* activation.

Effective free energy barriers for CO* activation without a vicinal CH* ($\Delta G_0^{\ddagger}$) and with a vicinal CH* ($\Delta G_1^{\ddagger}$) were determined using the RPBE method with PAW and with the D3 method employed for determining dispersive interaction energies between all atoms (RPBE-D3) and only between C, H, and O-atoms (RPBE-D3(NMI)), as reported in the 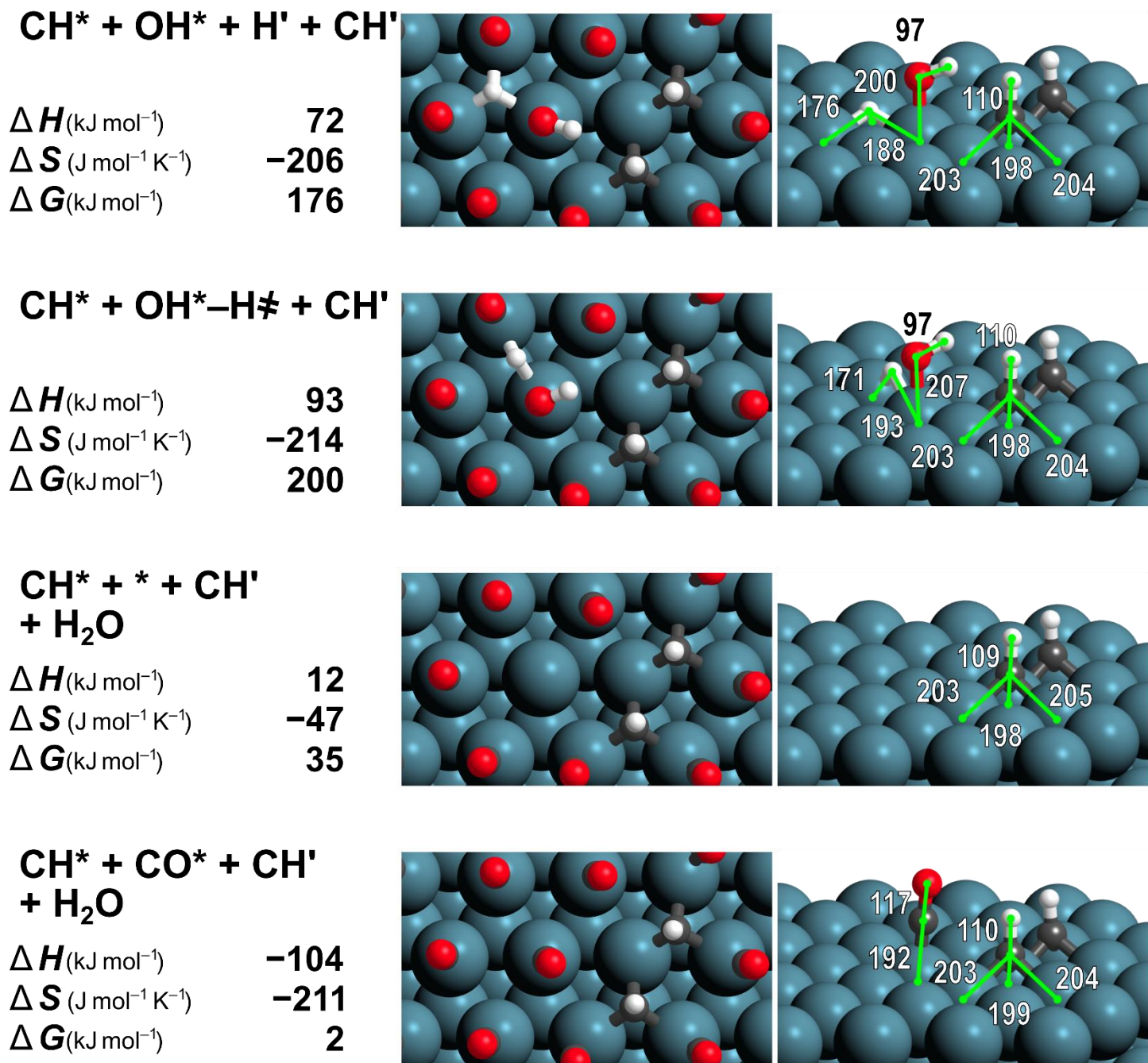main text. Furthermore, these effective free energy barriers ($\Delta G_0^{\ddagger}$ and $\Delta G_1^{\ddagger}$) were also computed using the PW-91 method (with USPP) and the optB86b-vdW method (with PAW) which explicitly includes dispersive vdW interactions within the functional. Figure S10 and Table R1 show the correlation between the difference in 'promoted' ($\Delta G_1^{\ddagger}$) and 'unpromoted' ($\Delta G_0^{\ddagger}$) free energy barriers for CO* activation and the adsorption free energy of CO* for all of these methods. Methods which correctly predict negative CO* adsorption free energies (consistent with large CO* coverages during FTS) will also lead to large promotional effects.

S4. Summary of DFT-derived reaction energies

Table S2. Reaction energetics (relative to CO* + CO* state) for H*-assisted CO* dissociation without vicinal chains.

Surface-Bound Species	Gas-Phase Species	ΔE_0	ΔE_{D3}	$\Delta E_{D3,NMI}$	$\Delta ZPVE$	ΔH_{vtr}	ΔG_{vtr}	ΔH	ΔG	$\Delta H_{D3,NMI}$	$\Delta G_{D3,NMI}$	ΔS
						kJ mol^{-1}						J mol^{-1} K^{-1}
CO* + CO*	1.5 H$_2$	**0**	**0**	**0**	**0**	**0**	**0**	**0**	**0**	**0**	**0**	**0**
CO* + *	CO, 1.5 H$_2$	**53**	**120**	**58**	**-8**	**-13**	**11**	**46**	**-36**	**104**	**22**	**165**
CO* + * + H'	CO, H$_2$	61	81	42	-3	-11	11	55	7	**97**	**50**	95
H–CO ⧸	CO, H$_2$	144	97	52	0	-14	17	137	98	**189**	**150**	77
HCO**	CO, H$_2$	125	86	51	5	-12	14	125	81	**176**	**131**	89
HCO + H'	CO, 0.5 H$_2$	137	50	33	11	-10	14	138	128	**172**	**162**	20
HCO–H ⧸	CO, 0.5 H$_2$	**211**	**63**	**29**	**4**	**-11**	**17**	**204**	**199**	234	228	**10**
HCOH	CO, 0.5 H$_2$	130	88	39	23	-10	15	143	134	**182**	**173**	18
HC–OH ⧸	CO, 0.5 H$_2$	197	76	30	16	-11	15	203	195	**233**	**225**	15
CH* + OH*	CO, 0.5 H$_2$	114	54	31	17	-7	9	124	106	**155**	**137**	36
CH* + OH* + H'	CO	135	14	13	24	-6	11	146	165	**159**	**178**	-39
CH* + H–OH* ⧸	CO	161	25	10	19	-8	15	165	190	**175**	**200**	-51
CH* + *	CO, H$_2$O	15	131	65	25	-19	20	31	-30	**95**	**34**	122
CH* + CO*	H$_2$O	-54	20	9	33	-6	9	-32	-11	**-23**	**-2**	-41

Table S3. Reaction energetics (relative to CH* + CO* state) for H*-assisted CO* dissociation vicinal to CH*.

Surface-Bound Species	Gas-Phase Species	ΔE_0	ΔE_D	$\Delta E_{D3,NMI}$	$\Delta ZPVE$	ΔH_{vtr}	ΔG_{vtr}	ΔH	ΔG	$\Delta H_{D3,NMI}$	$\Delta G_{D3,NMI}$	ΔS $J\ mol^{-1}\ K^{-1}$
CH* + CO*	1.5 H$_2$	**0**	**0**	**0**	**0**	**0**	**0**	**0**	**0**	**0**	**0**	**0**
CH* + CO* + H'	H$_2$	15	-31	-18	5	2	-1	15	49	**-2**	**31**	-68
CH' + *H–CO* ⧸	H$_2$	120	-38	-14	10	-2	6	120	164	**106**	**151**	-88
CH' + HCO**	H$_2$	74	-39	-17	16	1	2	83	121	**65**	**103**	-76
CH' + *HCO* + H'	0.5 H$_2$	93	-74	-35	23	2	2	103	176	**68**	**140**	-145
CH' + *HCO–H* ⧸	0.5 H$_2$	**162**	**-53**	**-36**	**15**	**1**	**6**	**163**	**240**	127	204	**-155**
CH' + *HCOH*	0.5 H$_2$	79	-47	-29	34	2	3	101	174	**72**	**145**	-147
CH' + *HC–OH* ⧸	0.5 H$_2$	156	-59	-40	25	3	2	169	241	**129**	**201**	-144
CH' + CH* + OH*	0.5 H$_2$	90	-66	-39	27	5	-1	108	174	**68**	**135**	-133
CH' + CH* + OH* + H'	--	109	-99	-56	35	6	0	129	232	**72**	**176**	-206
CH' + CH* + H–OH* ⧸	--	139	-92	-59	29	5	3	151	258	**93**	**200**	-214
CH' + CH* + *	H$_2$O	-4	2	-8	37	-7	10	20	43	**12**	**35**	-47
CH' + CH* + CO*	H$_2$O	-71	-114	-63	44	6	-1	-40	65	**-104**	**2**	-211

16

Table S4. Reaction energetics (relative to CH$_3$C* + CO* state) for H*-assisted CO* dissociation vicinal to CH$_3$C*.

Surface-Bound Species	Gas-Phase Species	ΔE_0	ΔE_D	$\Delta E_{D3,NMI}$	$\Delta ZPVE$	ΔH_{vtr}	ΔG_{vtr}	ΔH	ΔG	$\Delta H_{D3,NMI}$	$\Delta G_{D3,NMI}$	ΔS $J\ mol^{-1}\ K^{-1}$
CH$_3$C* + CO*	1.5 H$_2$	**0**	**0**	**0**	**0**	**0**	**0**	**0**	**0**	**0**	**0**	**0**
CH$_3$C* + CO* + H'	H$_2$	11	-37	-18	5	2	-1	11	44	**-7**	**26**	-67
CH$_3$C' + *H–CO* ⧸	H$_2$	134	-33	-16	10	-2	7	135	180	**119**	**165**	-91
CH$_3$C' + HCO**	H$_2$	93	-25	-19	17	0	5	102	144	**83**	**125**	-84
CH$_3$C' + *HCO* + H'	0.5 H$_2$	114	-61	-38	24	1	5	125	201	**86**	**163**	-152
CH$_3$C' + *HCO–H* ⧸	0.5 H$_2$	**178**	**-60**	**-39**	**15**	**1**	**6**	**178**	**257**	**139**	**217**	**-157**
CH$_3$C' + *HCOH*	0.5 H$_2$	97	-41	-32	35	2	4	118	193	**87**	**162**	-150
CH$_3$C' + *HC–OH* ⧸	0.5 H$_2$	157	-62	-40	25	2	6	169	246	**129**	**206**	-154
CH$_3$C' + CH* + OH*	0.5 H$_2$	99	-64	-41	27	5	-1	117	183	**75**	**142**	-133
CH$_3$C' + CH* + OH* + H'	--	107	-93	-58	34	6	2	124	230	**66**	**172**	-211
CH$_3$C' + CH* + H–OH* ⧸	--	141	-94	-61	27	5	4	151	260	**90**	**199**	-217
CH$_3$C' + CH* + *	H$_2$O	11	-2	-13	37	-8	11	35	60	**22**	**47**	-49
CH$_3$C' + CH* + CO*	H$_2$O	-74	-113	-64	43	5	0	-45	63	**-109**	**-1**	-215

Table S5. Reaction energetics (relative to $C_2H_5C^*$ + CO^* state) for H^*-assisted CO^* dissociation vicinal to $C_2H_5C^*$.

Surface-Bound Species	Gas-Phase Species	ΔE_0	ΔE_D	$\Delta E_{D3,NMI}$	$\Delta ZPVE$	ΔH_{vtr}	ΔG_{vtr}	ΔH	ΔG	$\Delta H_{D3,NMI}$	$\Delta G_{D3,NMI}$	ΔS $J\ mol^{-1}\ K^{-1}$
$C_2H_5C^*$ + CO^*	1.5 H_2	**0**	**0**	**0**	**0**	**0**	**0**	**0**	**0**	**0**	**0**	**0**
$C_2H_5C^*$ + CO^* + H'	H_2	18	-26	-19	7	1	3	18	56	**-1**	**37**	-76
C_2H_5C' + $^*H\text{–}CO^*$ ⧸	H_2	129	-19	-15	10	-2	7	130	176	**115**	**161**	-91
C_2H_5C' + HCO^{**}	H_2	92	-18	-19	16	0	5	101	143	**82**	**123**	-83
C_2H_5C' + $^*HCO^*$ + H'	0.5 H_2	97	-36	-36	22	2	3	107	180	**71**	**144**	-147
C_2H_5C' + $^*HCO\text{–}H^*$ ⧸	0.5 H_2	**172**	**-51**	**-38**	**12**	**1**	**7**	**171**	**249**	133	211	**-156**
C_2H_5C' + $^*HCOH^*$	0.5 H_2	81	-56	-31	32	3	4	101	176	**70**	**145**	-149
C_2H_5C' + $^*HC\text{–}OH^*$ ⧸	0.5 H_2	172	-66	-43	25	2	6	185	262	**142**	**219**	-155
C_2H_5C' + CH^* + OH^*	0.5 H_2	98	-53	-42	29	3	6	116	191	**74**	**150**	-151
C_2H_5C' + CH^* + OH^* + H'	--	117	-90	-59	35	5	5	135	245	**76**	**186**	-219
C_2H_5C' + CH^* + $H\text{–}OH^*$ ⧸	--	153	-90	-61	29	5	4	165	273	**104**	**212**	-216
C_2H_5C' + CH^* + *	H_2O	16	11	-13	37	-9	15	39	69	**26**	**56**	-60
C_2H_5C' + CH^* + CO^*	H_2O	-61	-107	-65	45	5	3	-31	80	**-96**	**15**	-222

Table S6. Reaction energetics (relative to $C_3H_7C^* + CO^*$ state) for H^*-assisted CO^* dissociation vicinal to $C_3H_7C^*$.

Surface-Bound Species	Gas-Phase Species	ΔE_0	ΔE_D	$\Delta E_{D3,NMI}$	$\Delta ZPVE$	ΔH_{vtr}	ΔG_{vtr}	ΔH	ΔG	$\Delta H_{D3,NMI}$	$\Delta G_{D3,NMI}$	ΔS $J\ mol^{-1}\ K^{-1}$
$C_3H_7C^* + CO^*$	1.5 H_2	**0**	**0**	**0**	**0**	**0**	**0**	**0**	**0**	**0**	**0**	**0**
$C_3H_7C^* + CO^* + H'$	H_2	19	-44	-22	6	1	1	19	55	**-2**	**34**	-72
$C_3H_7C' + {}^*H–CO^* \not{}$	H_2	134	-23	-14	10	-1	5	135	177	**121**	**163**	-86
$C_3H_7C' + HCO^{**}$	H_2	97	-18	-18	16	4	-8	110	134	**92**	**116**	-48
$C_3H_7C' + {}^*HCO^* + H'$	0.5 H_2	98	-38	-37	22	2	1	108	180	**71**	**143**	-144
$C_3H_7C' + {}^*HCO–H^* \not{}$	0.5 H_2	**183**	**-56**	**-39**	**14**	**1**	**4**	**183**	**258**	145	220	**-150**
$C_3H_7C' + {}^*HCOH^*$	0.5 H_2	85	-55	-30	31	3	2	105	177	**74**	**147**	-144
$C_3H_7C' + {}^*HC–OH^* \not{}$	0.5 H_2	175	-61	-44	25	6	-3	192	256	**148**	**212**	-128
$C_3H_7C' + CH^* + OH^*$	0.5 H_2	99	-60	-42	28	3	4	116	189	**74**	**147**	-147
$C_3H_7C' + CH^* + OH^* + H'$	--	117	-92	-59	35	5	5	136	244	**76**	**185**	-218
$C_3H_7C' + CH^* + H–OH^* \not{}$	--	155	-82	-62	28	8	-4	170	267	**108**	**205**	-194
$C_3H_7C' + CH^* + {}^*$	H_2O	18	13	-12	36	-8	14	40	69	**28**	**56**	-57
$C_3H_7C' + CH^* + CO^*$	H_2O	-59	-106	-65	45	5	2	-29	80	**-95**	**15**	-219

19

S5. Derivation of modified CO consumption rate equation

The total CO* consumption expression, including the vicinal CO-activation mechanism, is derived here based on Langmuir-Hinshelwood kinetics. In Scheme 1, CO* is consumed in the irreversible addition of the second H' to form the CH*OH* transition state, which can occur either next to a growing chain or in an unperturbed CO*-covered surface. The total CO* consumption rate in this process represents the sum of consumption near each length growing chain, which can be written as:

$$r_{CO} = k_{CHOH,0} K_{CHO,0}[CO^*][*][H']^2 + \sum_i \left(k_{CHOH,i} K_{CHO,i}[CO^*][C_i^*][H']^2 \right) \tag{S14}$$

where r_{CO} is the net rate of CO consumption, $k_{CHOH,0}$ is the CH*OH* formation activation rate constant with no growing chains nearby, $k_{CHOH,i}$ is the CH*OH* formation activation rate constant vicinal to a chain of length i, $[CO^*]$ represents CO surface concentration, $[*]$ represents vacant site surface concentration, and $[H']$ represents hydrogen surface coverage in *non-competitive adsorption* with carbon-based adsorbates.

By assuming that hydrogen undergoes non-competitive adsorption, the concentration of surface hydrogen can be related to the gas phase pressure by:

$$[H'] = [K_{H2}(H_2)]^{0.5} \tag{S15}$$

Assuming that CO* is the most abundant surface intermediate, and that CO* is quasi-equilibrated with the gas phase, the surface concentration of CO* and free sites * can be represented as:

$$[CO^*] = \frac{K_{CO}(CO)}{1+K_{CO}(CO)} \tag{S16}$$

$$[*] = \frac{1}{1+K_{CO}(CO)} \tag{S17}$$

Using an Anderson-Shulz-flory formalism, the concentration of any length growing chain can be related back to the concentration of C_1 chains and the chain growth probability using:

$$[C_n^*] = [C_1^*] \prod_{i=1}^{n} \alpha_{i-1} \tag{S18}$$

where the chain growth probability is defined as the rate of propagation of a growing chain:

$$\alpha_i = \frac{r_{growth,i}}{r_{growth,i}+r_{term,i}} \tag{S19}$$

and the rate constants governing CO-activation can be condensed into γ using:

$$\gamma_n = k_{HCOH,n} K_{HCO} K_{H2} \tag{S20}$$

By combining equations S14-S20, the net consumption of CO can be expressed as:

$$r_{CO} = \frac{\gamma_0 K_{CO}(CO)(H_2)}{[1+K_{CO}(CO)]^2} + \frac{K_{CO}(CO)(H_2)[C_1^*]\sum_{n=1}^{\infty}\gamma_n \prod_{i=1}^{n}\alpha_{i-1}}{1+K_{CO}(CO)} \qquad (S21)$$

The only surface concentration term in this equation is the concentration of C_1 growing chains. This quantity can be determined by employing the pseudo-steady-state-hypothesis on C_1 chains, where the net rate of generation can be expressed as:

$$r_{C1} = 0 = \frac{\gamma_0 K_{CO}(CO)(H_2)}{[1+K_{CO}(CO)]^2} - k_{methane}[C_1^*][K_{H2}(H_2)]^{1.5} - \frac{\gamma_1 K_{CO}(CO)(H_2)[C_1^*]}{1+K_{CO}(CO)} \qquad (S22)$$

The term reflecting the consumption due to methane can be eliminated by substituting the chain growth parameter for C1 chains, α_1, using:

$$\alpha_1 = \frac{\frac{\gamma_1 K_{CO}(CO)(H_2)[C_1^*]}{1+K_{CO}(CO)}}{\frac{\gamma_1 K_{CO}(CO)(H_2)[C_1^*]}{1+K_{CO}(CO)} + k_{methane}[C_1^*][K_{H2}(H_2)]^{1.5}} \qquad (S23)$$

By combining equation S22 and S23, the concentration of growing chains can be related to the concentration of vacant surface sites at steady state:

$$[C_1^*] = \frac{\gamma_0[*]\alpha_1}{\gamma_1} = \frac{\gamma_0 \alpha_1}{\gamma_1 [1+K_{CO}(CO)]} \qquad (S24)$$

Combining the result of equation S24 with the CO consumption equation in S21 yields:

$$r_{CO} = \frac{\gamma_0 K_{CO}(CO)(H_2)}{[1+K_{CO}(CO)]^2} + \frac{\gamma_0 \alpha_1 K_{CO}(CO)(H_2)\sum_{n=1}^{\infty}\gamma_n \prod_{i=1}^{n}\alpha_{i-1}}{\gamma_1[1+K_{CO}(CO)]^2} \qquad (S25)$$

which can be rearranged to yield the final expression:

$$r_{CO} = \frac{\gamma_0 K_{CO}(CO)(H_2)}{[1+K_{CO}(CO)]^2}\left(1 + \alpha_1 \sum_{n=1}^{\infty}\left(\frac{\gamma_n}{\gamma_1}\right)\prod_{i=1}^{n}\alpha_{i-1}\right) \qquad (S26)$$